Investigation of Material Deformation Mechanism in Double Side Incremental Sheet Forming

B. Lu[1, 2], Y. Fang[1], D.K. Xu[1,3], J. Chen[1]*, S. Ai·[1], H. Long[2], H. Ou[4], J. Cao[5]

[1] Department of Plasticity Technology, Shanghai Jiao Tong University, 1954 Huashan Rd, Shanghai, 200030, China

[2] Department of Mechanical Engineering, University of Sheffield, Sheffield, S1 3JD, UK

[3] State Key Laboratory of Development and Application Technology of Automotive Steels (Baosteel), Shanghai, 201900, P.R. China

[4] Department of Mechanical, Materials and Manufacturing Engineering, University of Nottingham, Nottingham, NG7 2RD, UK

[5] Department of Mechanical Engineering, Northwestern University, Evanston, IL 60208, USA

Abstract: Double side incremental forming (DSIF) is an emerging technology in incremental sheet forming (ISF) in recent years. By employing two forming tools at each side of the sheet, the DSIF process can provide additional process flexibility, comparing to the conventional single point incremental forming (SPIF) process, therefore to produce complex geometries without the need of using a backing plate or supporting die. Although this process has been proposed for years, there is only limited research on this process and there are still many unanswered open questions about this process. Using a newly developed ISF machine, the DSIF process is investigated in this work. Focusing on the fundamental aspects of material deformation and fracture mechanism, this paper aims to improve the understanding of the DSIF process. Two key process parameters considered in this study include the supporting force and relative position between master and slave tools. The material deformation, the final thickness distribution as well as the formability under varying conditions of these two process variables are investigated. An analytical model was developed to evaluate the stress state in the deformation zone. Using the developed model, an explicit relationship between the stress state and key process parameters was established and a drop of stress triaxiality was observed in the double contact zone, which explains the enhanced formability in the DSIF process. Based on the analytical and experimental investigation, the advancements and challenges of the DSIF process are discussed with a few conclusions drawn for future research.

Key words: double-sided incremental sheet forming; material deformation; formability; fracture.

Nomenclature:

a	Slave tool contact radius	ϕ	Forming angle
d	Distance from slave contact center	η	Stress triaxiality
F	Supporting force	κ	Contact condition parameter
k	major/minor strain ratio	μ	Friction coefficient
P_s	Contact pressure of slave tool	θ	Tangential contact angle
r_1	Master tool radius	$\tau_{r\theta}$	Tangential shear stress
r_2	Slave tool radius	$\bar{\sigma}$	Equivalent stress
t	Sheet thickness	σ_m	Hydrostatic stress
t_0	Initial sheet thickness	σ_r	Radial stress
ε_θ	Tangential strain	σ_θ	Tangential stress
ε_ϕ	Meridional strain	σ_ϕ	Meridional stress
ε_t	Thickness strain	σ_Y	Yield stress
$\bar{\varepsilon}$	Equivalent strain		

1. Introduction

Incremental sheet forming (ISF) is a highly versatile and flexible process for rapid manufacturing of complex sheet metal parts. This process has attracted an increasing interest in the field of sheet metal forming in the past decades due to its unique advantages including process flexibility, reduced tooling cost and increased material formability. Comparing to the conventional sheet forming processes, ISF has clear advantages in manufacturing of small batch or customized products. In the ISF process, localized plastic deformation takes place incrementally to ensure an improved material formability and therefore suitable for a wide range of sheet metal materials. During the past decades of the ISF technological development, various forms of ISF processes have been proposed. Iseki et al [1] developed the modern single point incremental forming (SPIF) process in late 1980s. A non-symmetrical part was first made based on a contour line tool path using a manually operated X-Y table. Matsubara [2] developed a two-point incremental forming (TPIF) process, in which the tool drew contours from inside to outwards while the blank holder gradually moves downwards on to a male die. Aiming to reduce the forming time and improve the sheet thickness distribution, Araghi et al [3] developed a hybrid process in which the stretch forming and non-symmetric incremental sheet forming were combined. Other processes such as laser-assisted incremental forming [4] and electricity-assisted incremental forming [5] have also been developed for processing difficult-to-form materials at elevated temperature. Other processes such as ISF using water jet has also been developed thus the direct metal-to-metal contact between tool and sheet can be avoided [6]. In addition, novel ISF tools including laser surface-textured (LST) tool [7] and an oblique roller ball (ORB) tool [8] have also been developed to improve the lubricant condition and to reduce friction between the tool-sheet contact surfaces. As a result of the continuous effort in the ISF development, sheet metal parts with complex shapes can be quickly formed using simple generic tools by developing geometry-specific tool paths.

In all ISF processes, the material plastic deformation occurs around the tool-sheet contact point because of the localized effects caused by the forming tool, such as bending-under-tension (BUT) and through thickness shear. These localized effects enhance the material deformation stability and suppress the development of material necking. In this way, the fracture forming limit diagram (FFLD), instead of the conventional forming limit curve (FLC), is used to evaluate the ISF formability. Concerning the fundamental aspects, the ISF material deformation mechanism has been investigated by many researchers. Emmens and Boogaard [9] found that the effect of continuous BUT is a critical factor to facilitate the localized material deformation and to achieve the

improved formability of ISF process. Through experiments, Eyckens et al [10] detected the existence of shearing deformation during ISF process by drilling small holes in the blank. Jackson and Allwood [11] demonstrated that the material deformation of ISF is due to the combination of bending, stretching and shearing by using experimental measurements in both SPIF and TPIF. Allwood and Shoulder [12] suggested that the through thickness shear is a significant factor to increase the sheet formability. Eyckens et al. [13] investigated the through thickness shear effect by using the Marciniak-Kuczynski model and suggested that this effect could enhance the formability. Eyckens et al. [14] also argued that the dominant material deformation mechanism, i.e. shearing or bending, depended on the specific process conditions, for example, bending is the dominant factor for the ISF of large wall angle cones. Hadoush et al. [15] suggested that the enhancement of deformation stability in the SPIF process was due to the tension and bending deformation, and the presence of compressive stress which improved the stability of the material deformation. Concerning the ISF modelling, Silva et al [16] presented an analytical model based on membrane approach to address the material deformation mechanism of ISF process and the effect of forming parameters on the ISF formability. Fang et al [17] established an analytical model to analyze the effects of bending and material hardening on the SPIF formability. In a recent research, Lu et al [8] investigated the effect of friction on the sheet deformation and fracture behavior in the ISF process. A 3D analytical model was developed with the consideration of the effect of friction. The above published literature identifies that the major SPIF deformation mechanism was a result of the combined deformation of bending, stretching and shearing, depending on process conditions.

In conventional ISF processes, whether it is SPIF, TPIF or hybrid forming processes, a single forming tool was usually used. Another emerging method is the double side incremental forming (DSIF), in which two forming tools are employed at each side of the sheet. In this way, greater process flexibility can be achieved and parts with both concave and convex features can be produced without a pre-prepared supporting die or backing plate. In the DSIF development, Meier et al [18] proposed a two point incremental forming process with two moving forming tools. Malhotra et al [19] developed an in-out toolpath strategy so that the continuous tool-sheet contact condition can be maintained. Another DSIF research was based on the electric pulse aided material deformation [20], in which the two tools acted as two electrodes. These studies demonstrated considerable potential of DSIF technology. Concerning the DSIF material deformation mechanism, the sheet deformation in the DSIF process may be different from those in the SPIF process when two tools act on both sides of the sheet. Limited study in the DSIF deformation mechanism has been reported in the literature. Among these, Meier et al

[21] theoretically and experimentally investigated the DSIF process. Smith et al [22] compared the difference of deformation mechanisms between conventional SPIF and the latest DSIF process. Both papers suggested that by squeezing the sheet using two forming tools, the formability of the material could be further improved due to the increased compressive pressure. Although these studies showed advantages of the DSIF process comparing to the conventional SPIF process, there are still a number of questions to be answered so as to provide an in-depth insight into the fundamental aspect of material deformation mechanics of the DSIF process. This is especially true for the role of two forming tools, the sheet deformation under double side compressive loading and the enhanced formability under the distributed hydrostatic stress causing by different tool squeezing effects.

Aiming to obtain a better understanding of the DSIF process, this paper focuses on more detailed investigation of the material deformation and fracture mechanism in the DSIF process. In this work, an analytical model has been developed based on the stress analysis of the sheet under the combined deformation of stretching, squeezing, bending and shearing. Stress triaxiality, as an indicator of the process formability, was evaluated to explain the fracture behavior under two key different forming parameters, i.e., the relative position of the master and slave tools and supporting force. In addition to the analytical study, experiments were also carried out to validate the analytical results and to further investigate the DSIF deformation mechanism and fracture behavior. Combining the analytical study and experimental observation, the unique material deformation and fracture mechanism in the DSIF process were discussed. The challenges of the DSIF process have also been identified, which is essential for the future development of this flexible sheet forming technology.

2. Stress Analysis of DSIF Process

The stress analysis is an efficient approach to improve the understanding in the material deformation of the incremental sheet forming process. Concerning the modeling approach of the conventional SPIF process, a few analytical models have been proposed, such as the work done by Silva [16, 23, 24], Fang [17] and Lu [8]. These models are based on either 3D or 2D plane strain analysis to explain the deformation and fracture mechanisms in the forming process. However, in the DSIF process, the stress state and the material deformation are even more complex due to the involvement of a slave tool. In this work, the stress analysis was performed to investigate the stress state in different deformation regions of the forming sheet. The definition of symbols used in the analysis is given in Nomenclature.

According to the geometric features in the deformation zone of the DSIF process, an analytical model was developed and illustrated in Fig. 1 (a) and (b). The master tool-sheet contact area is much larger than the slave tool-sheet contact area due to the convex contact between the master tool and the sheet. In this way, although a slave tool was employed in the DSIF process, the slave tool is only in contact with a partial region of the whole sheet deformation area. Depending on the contact condition and stress state, the deformation area can be split into the stretching zone and compression zone, respectively. The stretching zone is where the sheet only contacts with the master tool, which may be under tensile stress state as there is no additional squeezing from the slave tool. The compression zone is where the sheet contacts with both tools, which may be under compressive stress state as this region is squeezed by the master and slave tools. By considering a small element through the sheet thickness in the contact zone, as shown in Fig. 1(c), three stress components σ_r, σ_θ and σ_ϕ are defined along the directions of r, θ and ϕ, respectively. Concerning the shear stress, only the shear stress component $\tau_{r\theta}$ in the tool movement direction is considered whilst the other two shear stress components $\tau_{r\phi}$ and $\tau_{\theta\phi}$ are ignored as the two tools move mainly in the tangential direction. In the analysis, the shear stress $\tau_{r\theta}$ is determined by the frictional force caused by the two forming tools.
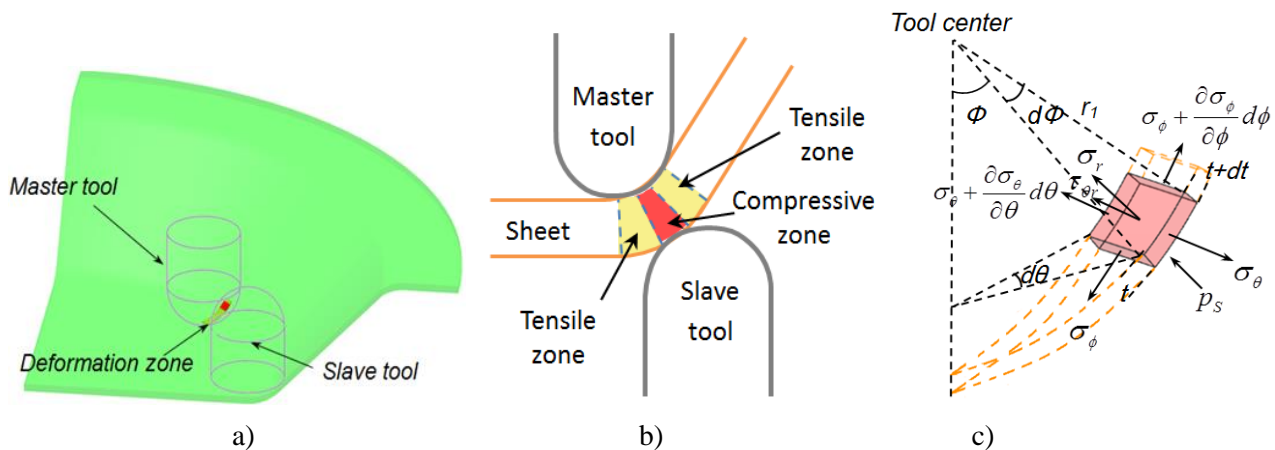
Fig. 1 – Analytical modeling of DSIF: a) Deformation area; b) Tensile and compressive zones; c) stress components

Based on the above analysis, the assumptions used in the analytical modeling of the DSIF can be summarized as follows:

(1) Membrane method is employed therefore no bending effect is considered in the analysis as the sheet is very thin comparing to the dimensions of the forming tool radii.

(2) Only the shear stress component in the tangential direction $\tau_{r\theta}$, along the tool movement direction, is considered therefore the other two shear stress components $\tau_{r\phi}$ and $\tau_{\theta\phi}$ are neglected.

(3) It is assumed that the radial stress component σ_r is independent of the tangential contact angle θ therefore the normal stress through thickness applied by tool pressure is evenly distributed along the tangential direction on the contact surface.

Considering the force equilibrant of the selected sheet element as shown in Figure 1 (c), along the tool movement direction, the equilibrant equation can be given by:

$$\sigma_\theta r_1 d\phi(t+\frac{dt}{2})\cos\frac{d\theta}{2} - \mu\sigma_r \cdot r_1 d\phi \cdot r_1 \sin\phi d\theta + \kappa \cdot \mu P_s \cdot (r_1+t+\frac{dt}{2})d\phi \cdot r_1 \sin\phi d\theta$$
$$= (\sigma_\theta + d\sigma_\theta)r_1 d\phi(t+\frac{1}{2}dt)\cos\frac{d\theta}{2} \tag{1}$$

where κ can be considered as a parameter to indicate the contact condition: in the double contact region, $\kappa = 1$; while in the single contact region, $\kappa = 0$. To determine the distribution of contact pressure P_s at the slave tool interface, Hertz contact equation of two spherical surfaces is employed [25], giving:

$$P_s(d) = \frac{3F}{2\pi a^2}\sqrt{1-\frac{d^2}{a^2}} \tag{2}$$

In this equation, a is related to the radius of the slave tool radius r_2 and other geometric parameters such as the curvature of outer surface of the sheet. This value may be directly measured in the experiment.

By neglecting the higher order terms, Eq. 1 can be simplified as:

$$d\sigma_\theta = -\frac{\mu\sin\phi}{t}[r_1 \cdot \sigma_r - \kappa \cdot (r_1+t)p_s]d\theta \tag{3}$$

As σ_r is assumed independent of θ, and the tangential stress is approximately zero i.e. $\sigma_\theta \approx 0$ at the boundary of contact zone ($\theta = 0$), using these boundary conditions, the tangential stress σ_θ can be given by:

$$\sigma_\theta = -\frac{\mu\sin\phi \cdot \theta}{t}[r_1\sigma_r - \kappa \cdot (r_1+t)P_s] \tag{4}$$

In the thickness direction, the equilibrant equation can be given by:

$$\sigma_r r_1 d\phi \cdot r_1 \sin\phi d\theta + \kappa \cdot P_s (r_1 + t + \frac{dt}{2}) d\phi \cdot r_1 \sin\phi d\theta$$

$$+\sigma_\theta r_1 d\phi (t + \frac{1}{2} dt) \cdot \sin\frac{d\theta}{2} \cdot \sin(\phi + \frac{1}{2} d\phi) + (\sigma_\theta + d\sigma_\theta) r_1 d\phi (t + \frac{1}{2} dt) \sin\frac{d\theta}{2} \cdot \sin(\phi + \frac{1}{2} d\phi) \quad (5)$$

$$+\sigma_\phi r_1 d\theta \cdot \sin\phi \cdot t \sin\frac{d\phi}{2} + (\sigma_\phi + d\sigma_\phi) r_1 d\theta \cdot \sin(\phi + d\phi) \cdot \sin\frac{d\phi}{2} (t + dt) = 0$$

which can be simplified as:

$$\frac{\sigma_r}{t} + \kappa \frac{r_1 + t}{r_1 t} P_s + \frac{\sigma_\theta}{r_1} + \frac{\sigma_\phi}{r_1} = 0 \quad (6)$$

Combining Eq.3 and Eq.6, it gives:

$$\sigma_\phi = (\mu \sin\phi \cdot \theta - 1) \frac{r_1}{t} \sigma_r - \kappa(1 + \mu \sin\phi \cdot \theta) \frac{r_1 + t}{t} P_s \quad (7)$$

Applying Tresca yield criterion, $\sigma_\phi - \sigma_r = \sigma_Y$, it gives:

$$\sigma_r = \frac{\sigma_Y}{(\mu \sin\phi \cdot \theta - 1)\frac{r_1}{t} - 1} + \kappa \frac{(1 + \mu \sin\phi \cdot \theta)(\frac{r_1}{t} + 1)}{(\mu \sin\phi \cdot \theta - 1)\frac{r_1}{t} - 1} P_s \quad (8)$$

Therefore, the hydrostatic stress of the contact zone can be calculated as:

$$\sigma_m = \frac{1}{3}(\sigma_\phi + \sigma_\theta + \sigma_r) = \frac{1}{3} \frac{\frac{r_1}{t} - 1}{1 + (1 - \mu \sin\phi \cdot \theta)\frac{r_1}{t}} \sigma_Y + \frac{\kappa}{3} \frac{\left(2\frac{r_1}{t} - 1\right)\mu \sin\phi \cdot \theta - 2}{1 + (1 - \mu \sin\phi \cdot \theta)\frac{r_1}{t}} \frac{r_1 + t}{t} \cdot P_s \quad (9)$$

Using Eqs 8 and 9, the stress triaxiality, η, at the single and double tool contact zone can be obtained:

$$\eta = \frac{\sigma_m}{\sigma_Y} = \frac{1}{3} \frac{\frac{r_1}{t} - 1}{1 + (1 - \mu \sin\phi \cdot \theta)\frac{r_1}{t}} + \frac{\kappa}{3} \frac{\left(2\frac{r_1}{t} - 1\right)\mu \sin\phi \cdot \theta - 2}{1 + (1 - \mu \sin\phi \cdot \theta)\frac{r_1}{t}} \frac{r_1 + t}{t} \cdot \frac{P_s}{\sigma_Y} \quad (10)$$

In tensile zone ($\kappa = 0$): $\quad \eta_s = \frac{1}{3} \frac{r_1 - t}{t + (1 - \mu \sin\phi \cdot \theta) \cdot r_1} \quad (11)$

In compressive zone ($\kappa = 1$): $\quad \eta_d = \eta_s + \gamma \cdot \frac{P_s}{\sigma_Y} \quad (12)$

where $\gamma = \frac{(2r_1 - t)\mu \sin\phi \cdot \theta - 2}{t + (1 - \mu \sin\phi \cdot \theta) \cdot r_1} \frac{r_1 + t}{3t}$ is a coefficient relating to the geometrical parameters and frictional

coefficient of the forming tools and the sheet. Eqs 11 and 12 indicate that the stress state in compressive zone can be considered as the tensile stress state plus an additional term that is influenced by the applied supporting force F and the material yield stress σ_Y.

As shown in Eq. (9), the hydrostatic stress varies with the actual thickness of the sheet t at different position of the deformation zone, which may be further expressed by the thickness strain component as:

$$t = t_0 e^{\varepsilon_t} \tag{13}$$

By neglecting the shear strain components, the equivalent strain $\bar{\varepsilon}$ can be given by:

$$\bar{\varepsilon} = \sqrt{\frac{2}{3}(\varepsilon_t^2 + \varepsilon_\theta^2 + \varepsilon_\phi^2)} \tag{14}$$

In the ISF process, it has been shown that the major strain may be considered as the meridional strain ε_ϕ while the minor strain may be considered as the tangential strain ε_θ [17]. The relationship of these two strain components may be given by a ratio, k:

$$\varepsilon_\theta = k\varepsilon_\phi \tag{15}$$

The ratio k may be determined by the sheet deformation state: while $k=0$, the deformation is under plane strain condition and while $k=1$, the deformation is under bi-axial stretching condition.

By considering the volume constant condition: $\varepsilon_t + \varepsilon_\theta + \varepsilon_\phi = 0$, the relationship between thickness strain and meridional strain can be given by:

$$\varepsilon_\phi = -\frac{\varepsilon_t}{(k+1)} \tag{16}$$

Using Eqs 15 and 16, the relationship between thickness strain and equivalent strain can be obtained as:

$$\varepsilon_t = -\frac{\sqrt{3}(k+1)}{2\sqrt{k^2+k+1}}\bar{\varepsilon} \tag{17}$$

Combining Eq.13 and 17, it gives

$$t = t_0 e^{-\frac{\sqrt{3}(k+1)}{2\sqrt{k^2+k+1}}\bar{\varepsilon}} \tag{18}$$

Thus the actual thickness can be represented by the equivalent strain, therefore Eqs 11 and 12 can be rewritten

as:

$$\text{Tensile zone:} \quad \eta_s = \frac{1}{3} \frac{r - t_0 e^{-\frac{\sqrt{3}(k+1)}{2\sqrt{k^2+k+1}}\bar{\varepsilon}}}{t_0 e^{-\frac{\sqrt{3}(k+1)}{2\sqrt{k^2+k+1}}\bar{\varepsilon}} + (1 - \mu \sin\phi \cdot \theta) \cdot r_1} \tag{19}$$

$$\text{Compressive zone:} \quad \eta_d = \eta_s + \gamma \cdot \frac{p_s}{\sigma_Y} \tag{20}$$

where

$$\gamma = \frac{(2r_1 - t_0 e^{-\frac{\sqrt{3}(k+1)}{2\sqrt{k^2+k+1}}\bar{\varepsilon}})\mu \sin\phi \cdot \theta - 2}{t_0 e^{-\frac{\sqrt{3}(k+1)}{2\sqrt{k^2+k+1}}\bar{\varepsilon}} + (1 - \mu \sin\phi \cdot \theta) \cdot r_1} \frac{r_1 + t_0 e^{-\frac{\sqrt{3}(k+1)}{2\sqrt{k^2+k+1}}\bar{\varepsilon}}}{3 t_0 e^{-\frac{\sqrt{3}(k+1)}{2\sqrt{k^2+k+1}}\bar{\varepsilon}}} \tag{21}$$

From Eq.19 it can be seen that the stress triaxiality in the tensile zone is related to the geometric parameters, r_1, θ and φ, the frictional coefficient μ, and the equivalent strain $\bar{\varepsilon}$. In the compressive zone, however, the stress triaxiality is further related to the material yield stress σ_Y and the contact force F.

Table 1 – SPIF and DSIF parameters used in the analytical calculation

Parameters	Value
Master tool radius r_1	5 mm
Support force F	240 N
Yield stress σ_Y	375 MPa
Forming angle ϕ	45°
Friction coefficient μ	0.1
tangential contact angle θ	10 °
Strain ratio k	0
Salve tool contact radius a	0.5 mm
Initial sheet thickness t_0	1 mm

Using Eqs (19) and (20), the distribution of stress triaxiality in relation to the equivalent strain $\bar{\varepsilon}$ can be determined. Using the assumed SPIF and DSIF parameters as given in Table 1, the distribution of stress triaxiality against the equivalent strain can be shown in Fig. 2. It can be seen that the difference between the SPIF and DSIF processes comes from the sudden drop of stress triaxiality at the double contact zone between both the master/slave tool and sheet.

(a) DSIF process   (b) SPIF process
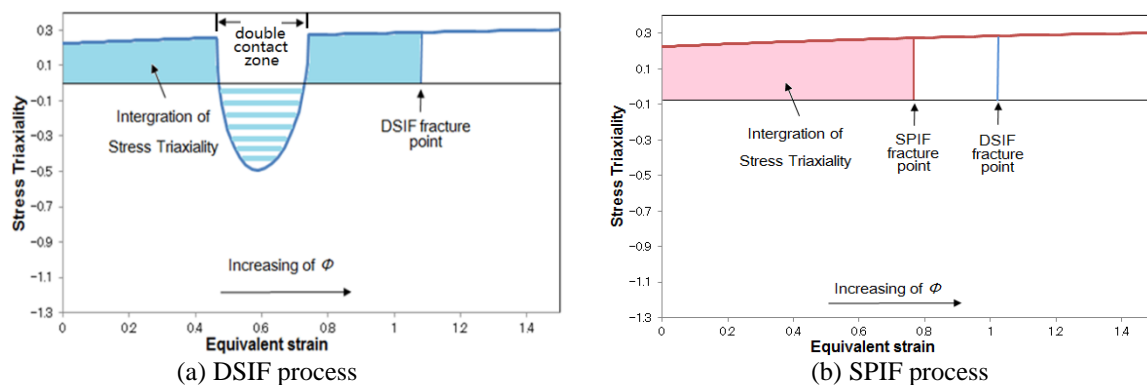
Fig. 2 - Comparison of stress triaxiality between SPIF and DSIF process: (a) DSIF; (b) SPIF

The stress triaxiality η is usually used to evaluate the formability in the incremental sheet forming process, such as in the work reported by Huang et al. [26], Silva et al. [24] and Lu et al [8]. The shaded areas in Fig. 2 represent the integration of stress triaxiality along the equivalent strain, which is a similar form of ductile fracture criteria, such as the Oyane fracture criterion [27]. When the shaded area is increased to a certain critical value during the deformation process, the material fracture occurs. As shown in Fig. 2, if the shaded areas in the SPIF and DSIF processes are the same, with the "stress drop", the fracture point in the DSIF process could achieve a greater strain value comparing to the SPIF process, which indicates the process capability to attain a greater material deformation and larger forming wall angle without fracture failure. This analogy explains the basic principle of the enhanced formability in the DSIF as compared to SPIF: the "stress drop" generated by the supporting force delays the fracture failure of material during deformation.

3 Experimental Design

The above analytical modeling describes the material deformation and fracture mechanism in the DSIF process. In order to validate the analytical model, a series of experiments are designed and conducted to examine the sheet deformation and fracture behavior in the DSIF process.

By reviewing previous study on the DSIF process, it has been concluded that major challenges come from the over squeezing or losing contact between the tool and sheet [19]. This may be caused by under or over prediction of sheet thinning, which leads to the inaccurate control of the gap between the two forming tools. In order to overcome this problem, Malhotra et al [19] proposed an in-out tool path strategy, which could overcome the problem of loss of contact. In this work, a different forming strategy was proposed by developing

a new DSIF concept without tool shift and with tool shift. As shown in Fig. 3, while the master tool is rigidly clamped and driven by the master XYZ linear motion unit, the slave tool is supported by an air cylinder, which acts as a spring to ensure the contact between the slave tool and sheet. By implementing this strategy, the rigid master tool guarantees the accurate position whilst the flexible slave tool can apply a supporting force on the sheet to ensure the sheet squeezing.

(a)   (b)
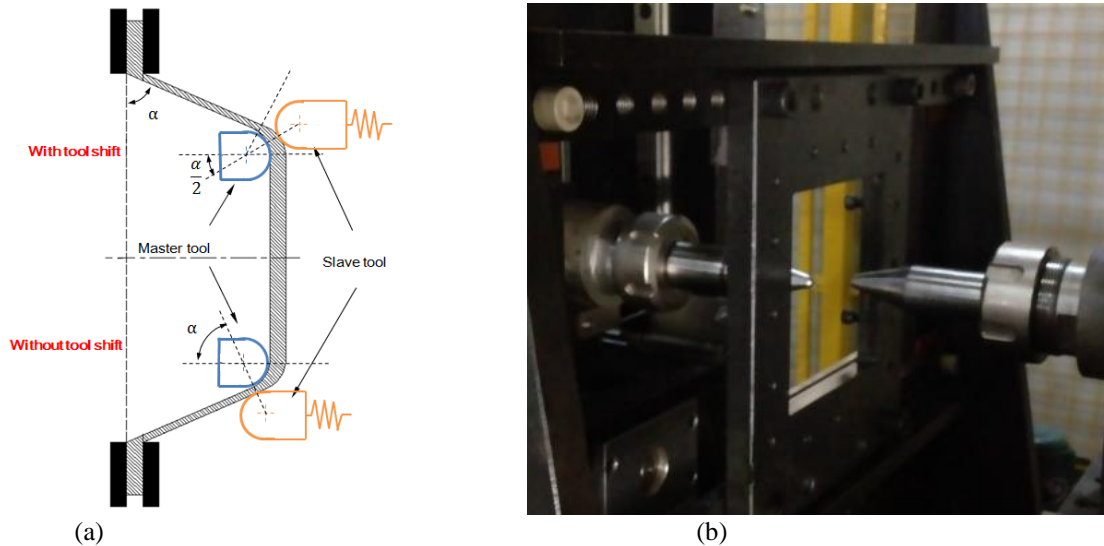
Fig. 3 – Developed DSIF concept: (a) without tool shift and with tool shift (b) developed DSIF machine

In the experiment, AA7075-T6 aluminum sheet with initial thickness of 1mm is used. The stress-strain curve of the sheet is obtained by tensile tests and is shown in Fig. 4. As can be seen, the material yield stress is about 375MPa. The elongation in the tensile test is about 8% due to the low strain hardening effect of the material. In the experiments, the radii of the master and slave tools are 5mm. A constant tool speed of 800mm/min is maintained for all testing cases. Solid lubricant MoS2 paste is used to reduce the friction between tools and sheet. The DSIF toolpaths are generated according to the designed forming geometry by using in-house developed software, in which the tool shift can be considered. In this work, the supporting force is varied in the range from 160N to 640N. These are empirical values based on the estimation of contact area [26] and the yield stress of the testing sheet, which ensures that the tool squeezing by itself would not cause the yielding of the sheet.
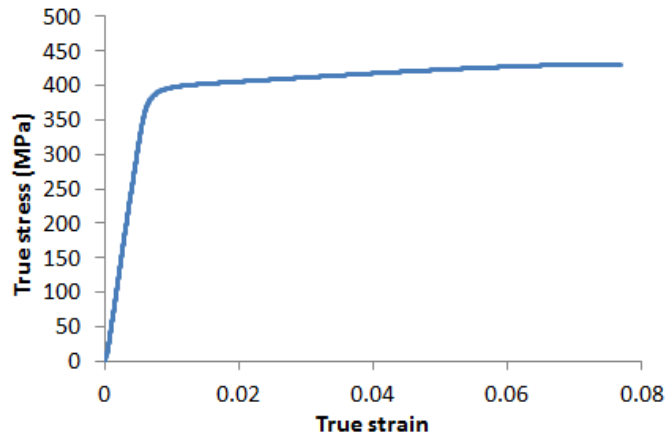
Fig.4 - The flow stress of AA7075-T6 sheet

In order to illustrate the material deformation and fracture mechanism as modeled in the analysis in Section 2, the hyperbolic cone with varying wall angle has been employed as shown in Fig. 5(a) and the cross sections of formed sheet part at both tangential and meridional direction are examined under two supporting force values of 240N and 480N with and without tool shift, respectively. In the experiment, the formability at various process conditions can be examined by the depth at which the fracture occurs in the forming process [28]. Varied values of the supporting force from 160N to 640N have been applied in the experiment while the tool shift has also been applied. In each case, the experiment is repeated three times and the average value is taken to ensure the repeatability of the results. In addition, a pyramid shape as shown in Fig. 5(b) is also employed to investigate the sheet deformation under the bi-axial stretching condition, from which the fracture forming limit diagram (FFLD) is derived to evaluate the effect of forming geometry on the DSIF formability.

(a)   (b)
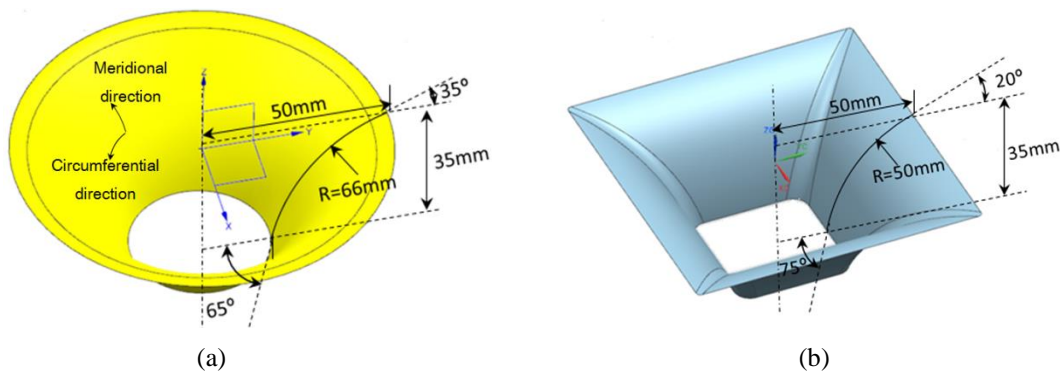
Fig. 5 –Tested DSIF geometries with variable wall angle: (a) Cone; (b) Pyramid

4 Results and Discussion

4.1 DSIF material deformation

To examine the sheet deformation behavior in the DSIF process, as shown in Fig. 6, small holes with a diameter

of 0.4 mm have been drilled in the sheet by using the micro electrical discharge machining (EDM) before DSIF processing. In order to reduce the local deformation caused by these drilled holes themselves, glue is used to fill the holes before the DSIF process. In this way, the localized deformation effect around the hole may be minimized. With the pre-drilled holes in the sheet, the deformation of the sheet can be examined by the final shape of the holes after deformation.
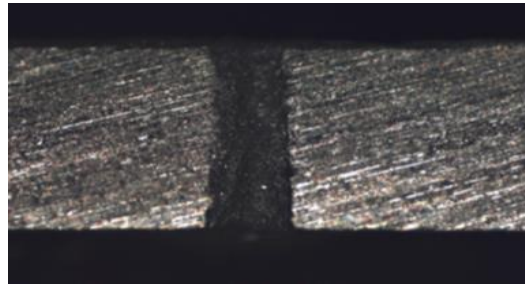
Fig. 6 – Sectional view of initial small hole on the sheet blank

The sheets with EDM holes are processed under different DSIF process conditions and the samples are prepared from the produced DSIF parts. The cross-sections of the holes in the tool movement direction are illustrated in Fig. 7. As can be seen in the Fig. 7, the through thickness shear in the tool movement direction can be observed for all the testing cases. This shear is independent of the tool position and value of the support force applied. The observed shear is similar to the that found in the SPIF process [8]. Concerning the sheet deformation, shearing can only be observed for the testing case without tool shift and supporting force of 240N, as shown in Fig. 7(a). While holding the supporting force constant in 240N, introducing the tool shift resulted in greater compressive deformation, as shown in Fig. 7(b). While the wall of the drilling hole, indicated by arrow A, remains as a straight line, however the wall indicated by arrow B is locally bended and becomes a concave shape. The difference in the deformation of wall A and B is not quite clear. It may be related to the combined effect from through thickness shear and squeezing. By increasing the supporting force to 480N from 240N as shown in Fig. 7(c), greater compressive deformation can be observed while the through thickness shear is less obvious. With both tool shift and increased supporting force, localized deformation of the hole can be observed as indicated by arrow C in Fig. 7(d) and the hole is almost closed at the surface of the slave tool side, indicating an even stronger squeezing effect. The observations on the deformed hole in the tool movement direction suggest that shifting the tool and increasing the supporting force will enhance the squeezing effect, which can even cause the closure of the hole.
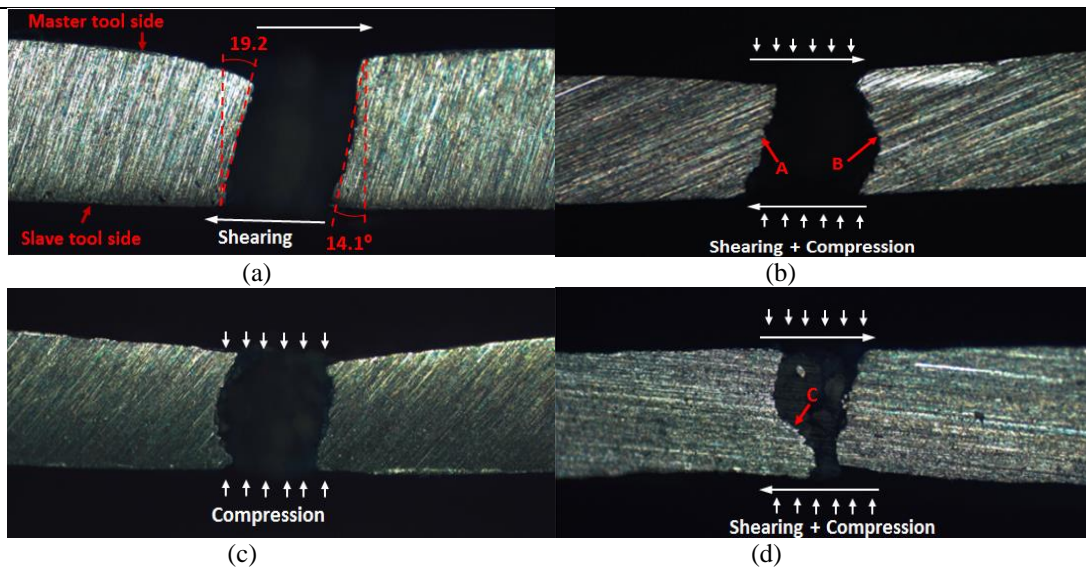
Fig. 7 – Material deformation in tangential cross-section of the hole: (a) 240N without tool shift; (b) 240N with tool shift; (c) 480N without tool shift; (d) 480N with tool shift

Fig. 8 shows the deformed cross-sections in the meridional direction under different DSIF process conditions. As can be seen, there is no obvious shear in this direction, which is consistent with the observations in the SPIF process [8]. In addition, under the low supporting force, no obvious squeezing can be observed and the major deformation occurred in this direction is stretching as shown in Fig.8 (a) and (b). By increasing the supporting force from 240N to 480N, the hole is significantly deformed or even closed in the case of applying tool shift, as shown in Fig. 8 (d). The observation in the meridional direction suggests that under low supporting force, the main deformation mode occurred in the meridional direction is stretching. However, under high supporting force, obvious tool squeezing is observed and the sheet deformation becomes stretching plus squeezing.
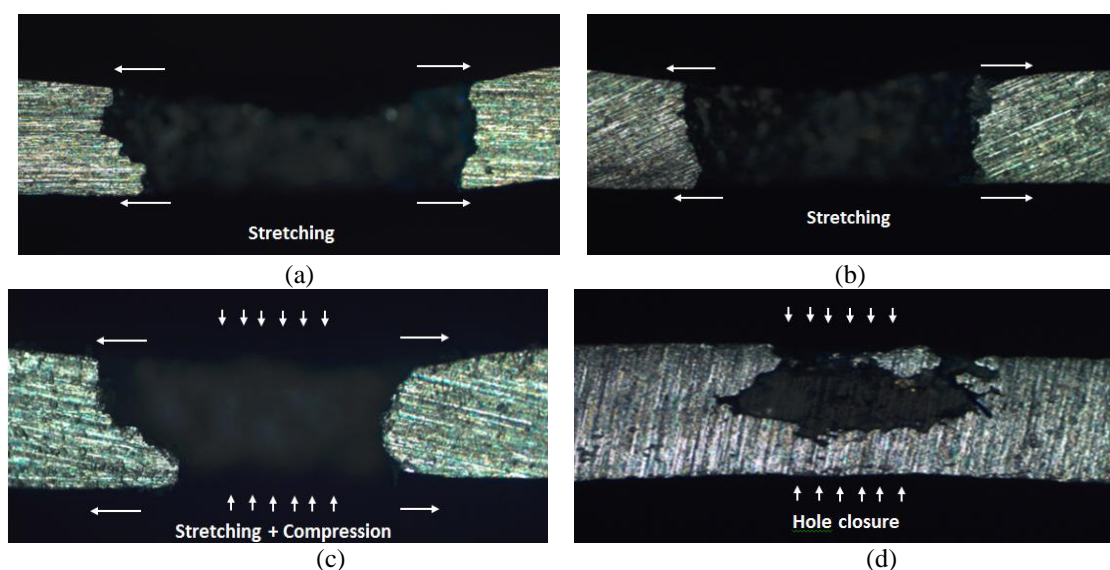
Fig.8 – Material deformation in meridional cross-section of the hole: (a) 240N without tool shift; (b) 240N with tool shift; (c) 480N without tool shift; (d) 480N with tool shift;

14

Considering the sheet deformation in both tool movement direction and meridional direction together, it can be concluded that the major deformation mode in the DSIF process is stretching in the meridional direction, compression in the radial direction and slight through thickness shear in the tool movement direction. Introducing the tool shift and increasing the supporting force have similar effect of increasing the compression. However it does not significantly affect the occurrence of the through thickness shear, as the contact area at slave tool side is smaller than that at the master tool side. This result also implies that the master tool still plays the major role than that of the slave tool in the DSIF material deformation.

4.2 The effect of supporting force on DSIF fracture

Tool squeezing is the most significant factor that differentiates the DSIF from the SPIF process. In order to study the effect of tool squeezing on the DSIF formability, a series of values of the supporting force is applied on the sheet by using the slave tool. The variations of fracture depth under different values of the supporting force are illustrated as Fig. 9(a). The evolution of fracture depth can be divided into three stages: at the first stage, when the supporting force is less than 240N, there is no significant change in the fracture depth and the tool squeezing does not make any obvious effect. At the second stage, when the supporting force is increased from 240N to 480N, the fracture depth increases from about 20mm to 30mm, which suggests that the tool squeezing has significantly enhanced the DSIF formality. By further increasing the supporting force up to 560N as illustrated in the third stage, the fracture depth starts to decrease. This   suggests that the tool squeezing is not a case of the larger the better: if the tool squeezing force is too high, it would have a negative impact on the formability. This is because the extremely high supporting force could bring some side effects as shown in Fig. 9(b): under the high support force of 560N, the two tools not only leave the observable marks on the sheet surface, but also clamp and stretch the sheet in the tool moving direction and resulted in the sheet fracture failure.
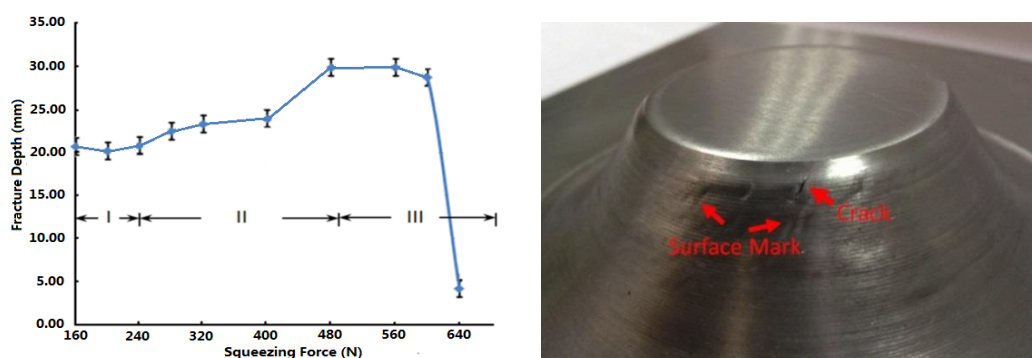
Fig. 9 – Effect of squeezing force: (a) Variation for forming depth under different supporting force; (b) Typical part formed under supporting force of 560N

The observation of the enhanced DSIF formability may be explained by using the developed stress analysis model. Using Eqs 19 and 20, the distribution of stress triaxiality along the deformation is obtained under two values of the supporting force of 240N and 480N, as shown in Fig. 10. It can be seen that an even greater "stress drop" occurs when the support force is increased from 240N to 480N. Greater supporting force further enhances the formability as the fracture point has moved further to the right of a greater equivalent strain due to a greater stress drop. In this way, higher degree of material deformation and a larger forming wall angle can be achieved without fracture failure. Fig. 10 explains the mechanism of enhanced formability due to the increase of the supporting force from the stress triaxiality point of view. However, the drop of formability under extremely high supporting force and stress triaxiality could not be explained because the effect from severe tool mark on formability is not considered in the analytical model.
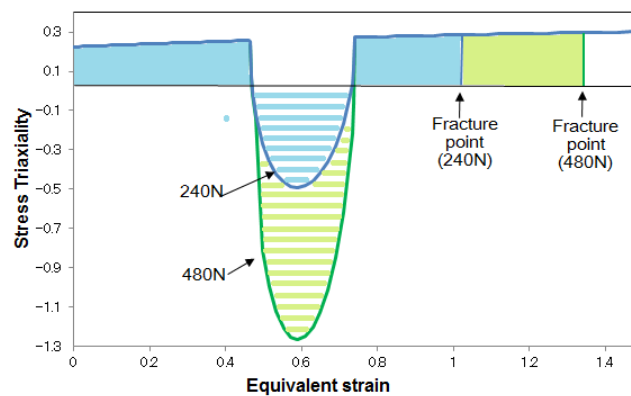
Fig. 10 - Effect of supporting force on stress triaxiality drop and DSIF formability

5.3 The effect of tool shift on DSIF fracture

The DSIF process provides additional flexibility on tool motion by introducing the slave tool. The relative position of the two tools is represented by the shift of slave tool. To investigate the influence of tool shift on the DSIF formability, the fracture depths in the testing cases with and without tool shift are examined under three levels of the supporting force at 240N, 400N and 480N. As shown in Fig. 11, under low supporting force of 240N, the formability in the case of tool shift is slightly lower than that without tool shift. However, with the increasing of supporting force, the tool shift shows a positive effect on the formability. In addition, it can be seen that the trend of formability variation with or without tool shift is different, where a rapid increase of formability at the enhanced squeezing effect can be obtained when tool shift is applied. For the cases without tool shift, the increase of formability is much slower. This result confirms the analytical assertion shown in Fig. 5 that the tool shift has a positive effect on DSIF formability.
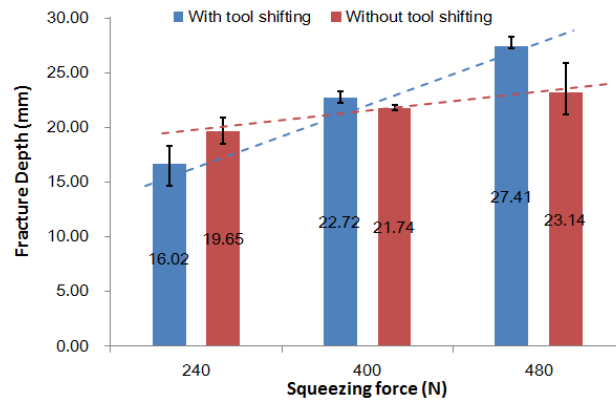
Fig. 11 – Influence of slave tool shift on DSIF formability

Fig. 12 further examines the effects of DSIF with and without tool shift on fracture. It is worth noting that the tool shift also affects the position of crack during the forming process. In both cases, the cracks occur in the single contact area rather than the double contact area, which suggests that the crack is initiated at the tensile deformation zone. For the case without tool shift, the crack is developed before the material reaches the double contact zone. For the case with tool shift, the crack occurs when the slave tool moves away from the contact region, which may be caused by the post-stretching of the master tool. By examining the case without tool shift, it can be found that the sheet is reversely bended due to the high supporting force. As shown in Fig. 12, this reverse bending may have a positive effect for enhanced formability. This evidence can be found in Fig. 11 in the cases with the supporting force of 240N. In the case with tool shift, there is no obvious reverse bending, but the supporting force causes the localized material deformation and left tool marks at the contact zone.
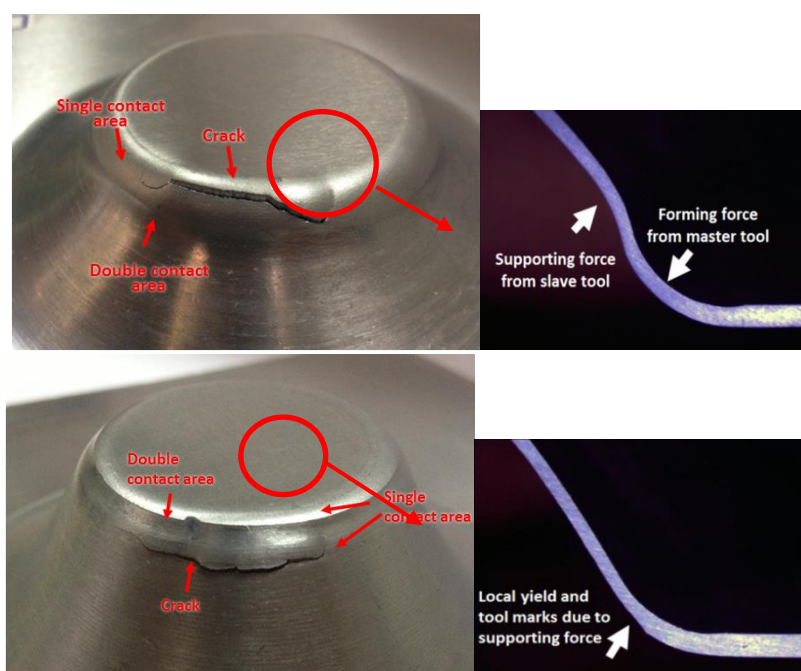
Fig. 12 – Localized material deformation with tool shift: a) Without tool shift; b) With tool shift

17

The effect of tool shift may be explained by the change of the location where the stress drop occurs using the developed analytical model. Fig. 13 compares the stress triaxiality distribution under different contact positions due to the shift of the slave tool. With tool shift, the contact position and the stress drop move towards to the left side of a smaller equivalent strain value where the deformation begins. Consequently, the deformation could reach the stress drop earlier than the case without tool shift. Thus by keeping the shaded areas the same, the cracks may occur even before reaching the double contact zone in the case without tool shift, while the fracture point with tool shift would move further to the right of a greater equivalent strain value due to the stress drop, indicating an enhanced formability. This result matches the observation shown in Fig.12: the crack is initialed before the sheet deformation reaches the double contact zone in the case without tool shift while the crack is initialed after the double contact zone in the case with tool shift.
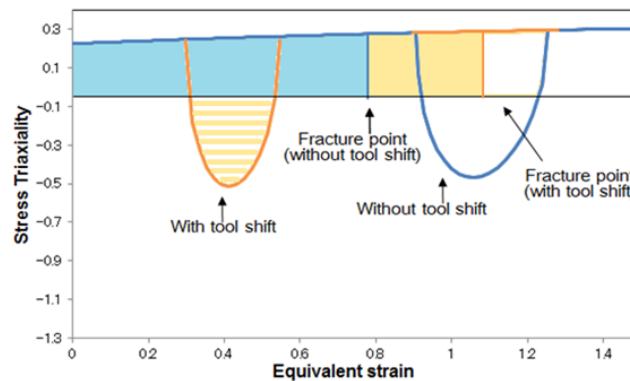
Fig. 13 - Effect of tool shift on the location of stress triaxiality drop and DSIF formability

5.4 Comparison of SPIF and DSIF formability

In addition to the use of the forming depth as an indicator of the DSIF formability, FFLD was also used to evaluate the formability for both SPIF and DSIF processes. In this study, both hyperbolic cone and pyramid parts were produced to demonstrate the effects of the plane-strain and bi-axial stretching deformation in the incremental forming process [29]. To evaluate strains at the occurrence of fracture, small circle grids with a diameter of 1mm were prepared on the sheet as shown in Fig. 14. By measuring the deformed ellipse after the DSIF processing, the strain values at fracture were determined.

(a) (b)
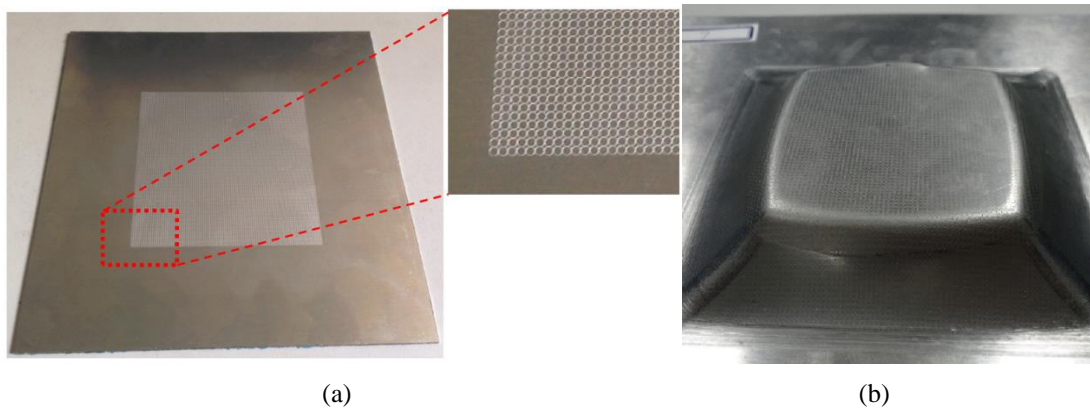
Fig. 14 – Fracture under different tool position: (a) Prepared sheet; (b) Formed part

Fig. 15 shows the FFLD for both SPIF and DSIF processes. It can be seen that the fracture forming limit obtained in the DSIF processes is always higher than that obtained from the SPIF process. By increasing the supporting force, the fracture forming limit can be increased. At the same time, by introducing the tool shift, the fracture forming limit can be further improved. Comparing with the deformation mode, it can be observed that the enhanced formability at the plane strain mode is more obvious than that at the bi-axial stretching mode.
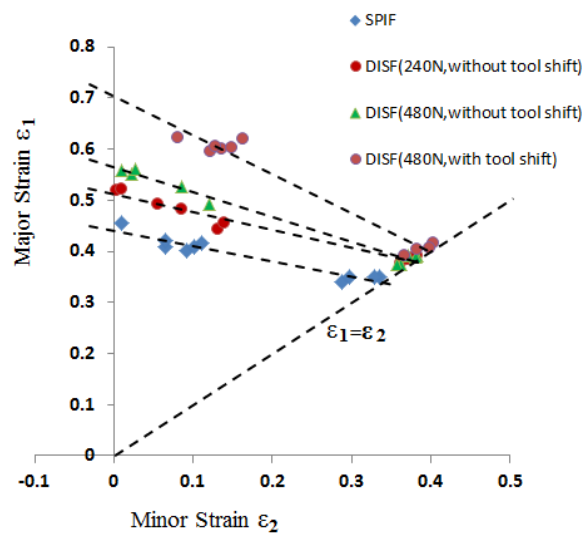
Fig. 15 – Fracture forming limit diagram under SPIF and DSIF process conditions

To understand the varied formability under both plane strain and bi-axial stretching deformation modes, different tangential contact angle θ and strain ratio k are employed. Under the plane strain condition, the assumption of the tangential contact angle of 10° and strain ratio of $k=0$ are made while under the bi-axial stretching condition, the tangential contact angle of 90° and strain ratio of $k=1$ are assumed. Under these conditions, the distributions of stress triaxiality are obtained as shown in Fig. 16. It can be observed that the "stress drop" in the bi-axial stretching condition is much smaller than those in plane strain condition. Comparing the supporting force, it can be found that increasing the supporting force would not significantly

affect the stress triaxiality under the bi-axial stretching condition comparing to the plane strain condition. This result explained the observation in Fig. 15 where the supporting force and tool shift are less effective in increasing the formability under the bi-axial stretching condition than that under the plane strain condition. Therefore, the strategy of using supporting force to increase the formability is more effective under plane strain condition. Or in other word, this strategy may be not effective in increasing the formability when forming a part with obvious corner features such as pyramid.
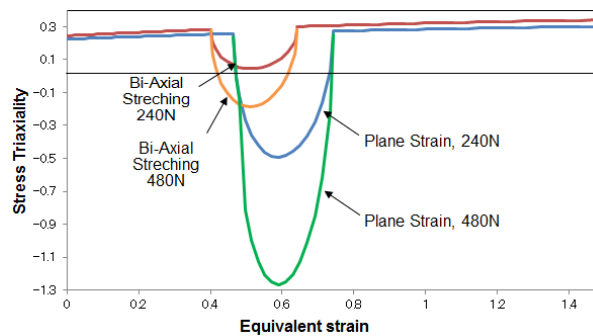
Fig. 16 - Effect of material deformation mode and supporting force on DSIF formability

5.5 Summary of results and discussion

The DSIF process concept developed in this study could significantly increase the process flexibility: the two tools could be positioned in different relative angles where different supporting forces can be applied. Additional support die or backing plate therefore becomes unnecessary. This work develops a different DSIF strategy comparing to previous research reported by Merier et al [18] and Cao et al [19]. In their work, the sheet was squeezed by predefined tool gap, a "squeezing by gap" strategy. In this work, the sheet was squeezed by predefined supporting force with a "squeezing by pressure" strategy. Concerning the advantages of the "squeezing by pressure" strategy, the problem of "losing contact between tool and sheet" in the conventional SPIF can be overcome. Although some novel strategies such as the "in-out" tool path have been developed [19], it may limit the potential of tool path variation. The advantage of "squeezing by pressure" approach developed in this work is that sheet squeezing can be well controlled and the defects such as "over squeezing" or "loss of contact" can be avoided. In this way, the DSIF process can be better controlled.

The increased flexibility in the DSIF process results in even more complex sheet deformation comparing to the SPIF process. The analytical model in this work suggests that the tool relative position and the supporting force employed in the DSIF process may cause varied stress states and the deformation zone of either tensile or compressive stress state. In the compressive zone, the "stress drop" would delay the material damage to reach

its critical value, which explains the increased formability in the DSIF process. The results obtained by the analytical model were further confirmed by the experimental results obtained in this work. However, concerning the limitation of the model, the experiment also shows that the supporting force and the stress triaxiality is not the larger the better. This phenomenon is not well explained by the analytical model as the effects of surface mark and tool stretching are not considered.

In addition to the analytical investigation, the experimental study suggests that comparing to the stretching, bending and shearing existing in the conventional SPIF process, additional squeezing effect introduced in the DSIF process plays a major role in material deformation. The tool squeezing and relevant sheet compression in the thickness direction, together with the stretching and bending, become the major deformation modes in the DSIF process.

Concerning the squeezing effect, by increasing the supporting force with or without shifting the tool relative positions, the DSIF formability can be enhanced as observed in Figs 10 and 11. However, there is a limit on enhanced formability: when the supporting force is too high, the formability decreases. This may be due to the excessively high contact pressure and stress triaxiality caused by the high supporting force. This observation is consistent with Hussain's recent work [30], in which the excessive high stress triaxiality could cause premature failure. In the DSIF case, under excessive high contact pressure and high friction, the two tools may "clamp" and "stretch" the sheet in the moving direction. This stretch may cause high tensile stress condition around the deformation zone and early failure of sheet. The analytical model could explain the DSIF fracture mechanism under normal stress triaxiality well but not under excessive stress triaxiality. Further efforts are required to improve the developed analytical model. Concerning the enhanced DISF formability, it shows great potential especially in processing difficult-to-form materials and the ability to combine with other techniques such as using electricity for local heating to further increase the formability. However, formability increase is more obvious under the plane-strain condition than under the bi-axial stretching condition as observed in the DSIF experiment in this work.

Concerning the bending effect, the experimental results obtained in this study suggest that reverse bending of the sheet may occur due to the slave tool pushing on the sheet. This reverse bending results in higher formability when the supporting force is not too high as shown in Fig. 14. This increased formability may be

explained by the enhanced bending-under-tension effect [31] and the increased deformation stability in DSIF process. However, when the supporting force is increased beyond a certain limit, the squeezing effect dominates the deformation of the sheet when this reverse bending effect becomes less significant. The reverse bending effect is not very clear at this stage and further investigation is needed in the future.

Concerning the shear deformation similar to SPIF process, the through thickness shear can be observed in the DSIF deformation. However, the shear effect may be overshadowed by the effect from squeezing and stretching in the DSIF process: the effect from shearing is not very obvious in the experiment comparing to those from squeezing. As also mentioned in previous work on investigation of the frictional effect in SPIF process [8], the shear deformation may not be the dominate deformation model in the incremental sheet forming process. The role of shear effect on the formability is still not quite clear. Further fundamental and systematic research on the shear effect is required.

This work has improved the understanding of the DSIF material deformation including stretching, squeezing, bending and shearing, and their combined effects on DSIF formability. It is worth mentioning that the DSIF process also provides high process flexibility with more degree of freedoms for the design of forming strategies than that in the conventional SPIF process. The tools could either move synchronously or independently at the same or different z-level. In addition, multi-pass forming strategies may also be applied in the DSIF process with specially designed intermediate sheet preforms. To achieve above forming strategies, robust tool path generation algorithms are indispensible to further explore the DSIF process flexibility in the future.

6 Conclusions

In this work, the material deformation and fracture mechanism of the developed DSIF concept, considering two key process parameters, supporting force and tool shift, have been investigated based on membrane stress analysis and experimental study. From this work, the following conclusions may be drawn:

1) In addition to the material deformation modes of stretching, bending and through thickness shear in the conventional SPIF process, the squeezing effect plays a major role in the DSIF process.

2) The tool squeezing and tool shift are the two key process parameters that affect the sheet deformation behavior and the formability in the developed DSIF concept.

3) By applying different levels of the supporting force and tool shift, the fracture forming limit can be increased to an even higher level than that by the SPIF process. However, this increase is more obvious for

forming geometries under the plane-strain condition rather than the double stretching condition.

4) The reverse bending generated in the DISF process without tool shift may also increase the formability when the supporting force is not too high.

5) The analytical model suggests that the tool squeezing results in a "stress drop", which delays the material deformation to reach the critical fracture point. The variations of supporting force and tool shift influence the DSIF formability through the change of the slave tool position and the magnitude of the "stress drop".

Acknowledgements

References

[1] H. Iseki, K. Kato, S. Sakamoto, Flexible and incremental sheet metal forming using a spherical roller, In: Proc. 40th JJCTP, (1989) 41–44 (in Japanese).

[2] S. Matsubara, Incremental Backward Bulge Forming of a Sheet Metal with a Hemispherical Head Tool, Journal of the J.S.T.P., 35 (1994) 1311-1316.

[3] B.T. Araghi, G.L. Manco, M. Bambach, G. Hirt, Investigation into a new hybrid forming process: Incremental sheet forming combined with stretch forming, CIRP Annals - Manufacturing Technology, 58 (2009) 225-228.

[4] J.R. Duflou, B. Callebaut, J. Verbert, H. De Baerdemaeker, Laser Assisted Incremental Forming: Formability and Accuracy Improvement, CIRP Annals - Manufacturing Technology, 56 (2007) 273-276.

[5] G. Fan, L. Gao, G. Hussain, Z. Wu, Electric hot incremental forming: A novel technique, International Journal of Machine Tools and Manufacture, 48 (2008) 1688-1692.

[6] B. Jurisevic, K. Kuzman, M. Junkar, Water jetting technology: an alternative in incremental sheet metal forming, The International Journal of Advanced Manufacturing Technology, 31 (2005) 18-23.

[7] D. Xu, W. Wu, R. Malhotra, J. Chen, B. Lu, J. Cao, Mechanism investigation for the influence of tool rotation and laser surface texturing (LST) on formability in single point incremental forming, International Journal of Machine Tools and Manufacture, 73 (2013) 37-46.

[8] B. Lu, Y. Fang, D.K. Xu, J. Chen, H. Ou, N.H. Moser, J. Cao, Mechanism investigation of friction-related effects in single point incremental forming using a developed oblique roller-ball tool, International Journal of Machine Tools and Manufacture, 85 (2014) 14-29.

[9] W.C. Emmens, A.H. Boogaard, Incremental forming by continuous bending under tension—An experimental investigation, Journal of Materials Processing Technology, 209 (2009) 5456-5463.

[10] P. Eyckens, A. Van Bael, R. Aerens, J. Duflou, P. Van Houtte, Small-scale finite element modelling of the plastic deformation zone in the incremental forming process, in: In Proceedings Esaform 2008, Lyon, France, April 23–25, 2008, pp. Paper 333.

[11] K. Jackson, J. Allwood, The mechanics of incremental sheet forming, Journal of Materials Processing Technology, 209 (2009) 1158-1174.

[12] J.M. Allwood, D.R. Shouler, Generalised forming limit diagrams showing increased forming limits with non-planar

stress states, International Journal of Plasticity, 25 (2009) 1207-1230.

[13] P. Eyckens, A. Van Bael, P. Van Houtte, Marciniak–Kuczynski type modelling of the effect of Through-Thickness Shear on the forming limits of sheet metal, International Journal of Plasticity, 25 (2009) 2249-2268.

[14] P. Eyckens, B. Belkassem, C. Henrard, J. Gu, H. Sol, A. Habraken, J. Duflou, A. Bael, P. Houtte, Strain evolution in the single point incremental forming process: digital image correlation measurement and finite element prediction, International Journal of Material Forming, 4 (2011) 55-71.

[15] A. Hadoush, A. Boogaard, W.C. Emmens, A numerical investigation of the continuous bending under tension test, Journal of material Processing Technology, 211 (2011) 1948-1956.

[16] M.B. Silva, M. Skjoedt, P.A.F. Martins, N. Bay, Revisiting the fundamentals of single point incremental forming by means of membrane analysis, International Journal of Machine Tools and Manufacture, 48 (2008) 73-83.

[17] Y. Fang, B. Lu, J. Chen, D.K. Xu, H. Ou, Analytical and experimental investigations on deformation mechanism and fracture behavior in single point incremental forming, Journal of Materials Processing Technology, 214 (2014) 1503-1515.

[18] H. Meier, V. Smukala, O. Dewald, J. Zhang, Two Point Incremental Forming with Two Moving Forming Tools, Key Engineering Materials, 344 (2007) 599-605.

[19] R. Malhotra, J. Cao, F. Ren, V. Kiridena, C. Xia, N. Reddy, Improvement of Geometric Accuracy in IncrementalForming by Using a Squeezing Toolpath Strategy with Two Forming Tools, Journal of Manufacturing Science and Engineering, 133 (2010) 603-611.

[20] J. Asgar, R. Lingam, N.V. Reddy, Tool path influence on electric pulse aided deformation during incremental sheet metal forming in: The 9th International Conference and Workshop on Numerical Simulation of 3D Sheet Metal Forming Prcesses, Melbourne, Australia, 2014, pp. 840-843.

[21] H. Meier, B. Buff, R. Laurischkat, V. Smukala, Increasing the part accuracy in dieless robot-based incremental sheet metal forming, CIRP Annals - Manufacturing Technology, 58 (2009) 233-238.

[22] J. Smith, R. Malhotra, W.K. Liu, J. Cao, Deformation mechanics in single-point and accumulative double-sided incremental forming, The International Journal of Advanced Manufacturing Technology, 69 (2013) 1185-1201.

[23] M. Silva, P. Nielsen, N. Bay, P.A.F. Martins, Failure mechanisms in single-point incremental forming of metals, The International Journal of Advanced Manufacturing Technology, 56 (2011) 893-903.

[24] M.B. Silva, M. Skjoedt, N. Bay, P.A.F. Martins, Revisiting single-point incremental forming and formability/failure diagrams by means of finite elements and experimentation, The Journal of Strain Analysis for Engineering Design, 44 (2009) 221-234.

[25] K.L. Johnson, Contact mechanics, Cambridge University Press, Cambridge, UK, 1985.

[26] Y. Huang, J. Cao, S. Smith, B. Woody, J. Ziegert, M. Li, Studies of size effect on the formability of a domed part in incremental forming, in: In Proceedings of the 2008 International Manufacturing Science and Engineering Conference, Illinois, USA, 2008.

[27] M. Oyane, T. Sato, K. Okimoto, S. Shima, Criteria for ductile fracture and their applications, Journal of Mechanical Working Technology, 4 (1980) 65-81.

[28] G. Hussain, L. Gao, A novel method to test the thinning limits of sheet metals in negative incremental forming, International Journal of Machine Tools and Manufacture, 47 (2007) 419-435.

[29] G. Hussain, N. Hayat, G. Lin, Pyramid as test geometry to evaluate formability in incremental forming: Recent results, J Mech Sci Technol, 26 (2012) 2337-2345.

[30] K.A. Al-Ghamdi, G. Hussain, Threshold tool-radius condition maximizing the formability in SPIF considering a variety of materials: Experimental and FE investigations, International Journal of Machine Tools and Manufacture, 88 (2015) 82-94.

[31] W.C. Emmens, Boogaard, A.H., Tensile tests with bending: a mechanism for incremental forming, International Journal of Material Forming, 1 (2008) 1155-1158.